COLLIDER PHYSICS : LHC

F. Gianotti
EP Division, CERN, Geneva, Switzerland

Abstract
The CERN Large Hadron Collider (LHC) will become operational in 2005. These lectures describe the physics motivations for the LHC, the experimental challenges, and the two general-purpose pp detectors (ATLAS and CMS). A few examples of the physics goals of these experiments are discussed: searches for Higgs boson(s) and Supersymmetric particles, and precise measurements of the W and top masses.

1. INTRODUCTION

The CERN Large Hadron Collider [1] is presently under construction and will start operation in 2005. This machine will be installed in the existing LEP tunnel and will provide pp collisions and heavy-ion (e.g. Pb-Pb) collisions. When running in pp mode, the centre-of-mass energy will be 14 TeV, which is a factor of about seven larger than at the present machine with the highest centre-of-mass energy (the Tevatron Collider at Fermilab), and the design luminosity will be 10^{34} cm^{-2}s^{-1}, which is a factor of about 100 larger than at previous machines (LEP, Tevatron). Such luminosity and centre-of-mass energy will allow searches for new particles to be performed up to masses of ~ 5 TeV.

The limiting factor to the achievable centre-of-mass energy is the bending power needed to keep the beams circulating in the 27 Km circumference of the LEP tunnel. From the equation

$$p(\mathrm{TeV}) = 0.3B(\mathrm{Tesla})R(\mathrm{Km})$$

where p is the beam momentum, B the magnetic field provided by the magnets of the machine and $R \simeq 4.3$ Km is the radius of the LEP ring, one can deduce that the bending power needed to achieve a beam momentum p = 7 TeV is about 5.4 Tesla. In practice, since the machine can not be completely filled with magnets, the needed bending power is obtained with about 1200 superconducting dipoles providing a field of 8.4 Tesla, which represents a very ambitious technological challenge.

Two phases are foreseen for the LHC operation: in the years 2005–2008 the instantaneous luminosity will start with 10^{33} cm^{-2}s^{-1} (the so-called 'low luminosity' phase) and will reach 10^{34} cm^{-2}s^{-1}, the design luminosity of the machine, afterwards ('high luminosity' phase). More details about the machine can be found in Ref. [1].

Four large-scale experiments will operate at the LHC. ATLAS [2] and CMS [3] are general-purpose pp experiments with a broad physics programme, including both searches for new particles and precision measurements. LHCb [4] is an experiment dedicated to the physics of B-hadrons and to CP-violation. ALICE [5] is a heavy-ion experiment which will study the behaviour of the nuclear matter at very high energies and densities, and in particular will explore the formation of the quark-gluon plasma. The physics potential of LHCb and ALICE are discussed in Ref. [6] and Ref. [7] respectively. Therefore these lectures concentrate on the ATLAS and CMS experiments.

2. MOTIVATIONS FOR THE LHC

The LHC is an unprecedented project, not only in terms of centre-of-mass energy and luminosity of the colliding beams, but also in terms of cost, complexity and size of the experiments, and human effort (the four collaborations involve more than 4000 physicists). It is supported by strong physics motivations, which are briefly discussed below.

- *Understand the origin of the particle masses*. Despite the success of the Standard Model (SM), whose predictions have been verified at the level of 0.1% or better by the LEP, SLC and Tevatron experiments, some aspects of the theory are still obscure. In particular, the origin of the particle masses, and the motivation for the mass hierarchy of leptons, quarks and gauge bosons, which apparently follows a random pattern, are not known. In the Standard Model, the Higgs mechanism provides a way to break the electroweak symmetry and to endow particles with masses.
  As a consequence of this mechanism, a scalar particle, the Higgs boson, is predicted, whose mass is not specified by the theory but which should not exceed 1 TeV to preserve unitarity at high energy. Such a particle has not been found yet and the present lower limit on its mass from the LEP experiments is about 108 GeV [8]. If the Higgs boson will not be found at LEP or at the Tevatron Run 2, this lower limit could be extended up to ~ 120 GeV.
  Therefore a new machine is needed to explore the mass range from ~ 120 GeV up to the theoretical upper bound of 1 TeV. As discussed in Section 7., the LHC experiments will be able to observe a SM Higgs boson over this full mass range.
- *Look for physics beyond the Standard Model*. There are several reasons to believe that the Standard Model is not the ultimate theory of particle interactions [9]. First, the Higgs mechanism has little physical justification and leads to divergent radiative corrections to the Higgs boson mass unless fine-tuned cancellations occur [9].
  Furthermore, there are hints that the coupling constants of the electromagnetic, weak and strong interactions, which run with energy as experimentally verified over the presently accessible energy range, could unify into a single value α_G at a very high energy scale ($\sim 10^{16}$ GeV). This possibility, which is predicted by Grand Unified Theories (GUT, [9]), is very attractive, because beyond the unification scale physics becomes simple: only one force exists with strength α_G. In the Standard Model, the coupling constants, as extrapolated from the experimentally measured values up to very high energy, fail to meet at a single point (see top plot of Fig. 1). On the other hand unification succeeds in more general theories, like Supersymmetry (SUSY), as shown in the bottom plot of Fig. 1. Therefore a machine is needed to look for manifestations of these theories, some of which predict new physics at an energy scale ($\sim$ TeV) accessible to the LHC.
- *Answer to many other open questions*. There are many other issues that the LHC could clarify. For instance, are quarks and leptons elementary particles ? Are there additional families of quarks, leptons and gauge bosons ? What is the origin of the asymmetry between matter and antimatter in the universe ? What is the origin of the QCD confinement and can quarks and gluons be deconfined in a plasma of quarks and gluons as in the early stages of the universe ? Etc..
- *Perform precision measurements*. Measuring as many properties as possible of the known particles and interactions with the highest possible precision is a complementary approach to direct searches to look for something new: any observed deviation from the Standard Model expectations is a signal of new physics.
  At the LHC, known particles such as W and Z bosons, top and b-quarks will be produced with huge rates, given the high energy and luminosity of the machine. Therefore, thanks to the large statistics of the data samples, many precise measurements will be possible, despite the harsh environment (see Section 4.). In most cases, the precision will be limited by systematic uncertainties. Whereas the parameters of the Z boson have been measured with unbeatable accuracy at SLD and LEP, improvements in many measurements related to W physics, Triple Gauge Couplings (i.e. couplings of the type WWγ and WWZ), b-quark and top-quark physics are expected at the LHC.

3. PHENOMENOLOGY OF PROTON-PROTON COLLISIONS

The total inelastic proton-proton cross-section is about 80 mb at $\sqrt{s}$ = 14 TeV. Therefore, the event rate R, defined as the number of events produced per second by the pp interactions, is expected to be

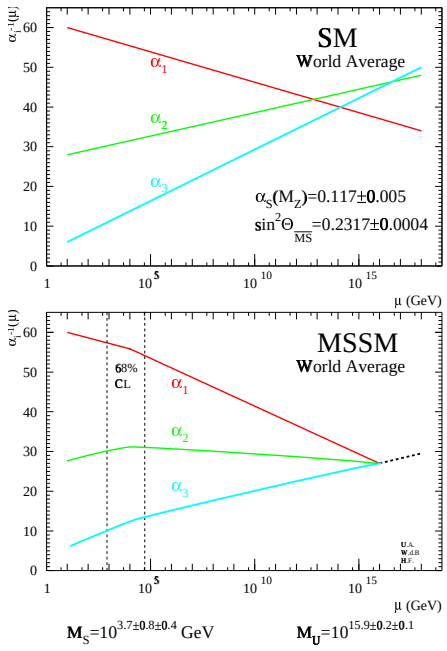

Fig. 1: Evolution of the coupling constants of the electromagnetic (α_1), weak (α_2) and strong (α_3) interactions with energy, as predicted by the Standard Model (top) and by Supersymmetry (bottom). Both plots are from Ref. [10].

$$R = \sigma \times L = 80 \text{ mb} \times 10^{34}\text{cm}^{-2}\text{s}^{-1} \simeq 10^9/\text{s}$$

when running at high luminosity. These events belong to two classes:

- Most events are due to large-distance collisions between the two incoming protons. In this case the momentum transfer of the interaction is small ('soft collisions') and therefore particle scattering at large angle is suppressed. The particles produced in the final state of such interactions have large longitudinal momentum, but small transverse momentum (p_T) relative to the beam line ($<p_T> \simeq 500$ MeV). Most of the collision energy escapes down the beam pipe.
  The final states arising from these soft interactions are called 'minimum bias' events. They represent by far the majority of the pp collisions but they are not interesting.
- Monochromatic proton beams can be seen as beams of partons (quarks and gluons) with a wide band of energy, as illustrated in Fig. 2. Occasionally, head-on collisions occur between two partons of the incoming protons. These are interactions at small distances, and therefore are characterised by large momentum transfers ('hard scattering'). In this case, particles in the final state can be produced at large angles with respect to the beam line (high p_T) and massive particles can be created.
  These are the interesting physics events. They are, however, rare compared to the soft interactions. For instance, the production of a W boson through the annihilation of a quark-antiquark pair has a cross-section of ∼150 nb, i.e. 10^5 times smaller than the total inelastic pp cross-section.

In the hard-scattering interactions of quarks and gluons at a hadron collider, the effective centre-of-mass energy of the interaction ($\sqrt{\hat{s}}$) is, unlike at e^+e^- colliders, smaller than the centre-of-mass energy of the machine ($\sqrt{s}$) and is given by:

$$\sqrt{\hat{s}} = \sqrt{x_a x_b s}$$

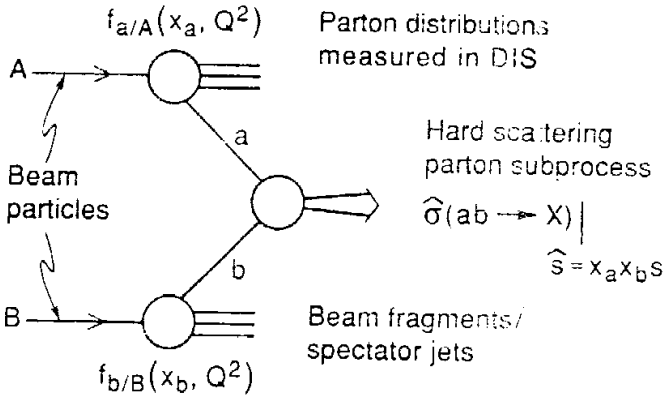

Fig. 2: Schematic representation of a high-p_T pp interaction.

where x_a and x_b are the fractions of the proton momentum carried by the two colliding partons (see Fig. 2). If $x_a \simeq x_b$, then the above relation becomes

$$\sqrt{\hat{s}} \simeq x\sqrt{s}$$

Therefore, in order to produce a particle of mass 100 GeV, two quarks (or gluons) which carry only 1% of the proton momentum are needed ($x \sim 0.01$), whereas a particle of mass 5 TeV can only be produced if two partons with $x \sim 0.35$ interact. The momentum distributions of quarks and gluons inside the proton are called parton distribution functions. An example of such a distribution is shown in Fig. 3. Up and down quarks contribute to the quantum numbers of the protons ('valence quarks') and therefore carry a large fraction of the proton momentum. Figure 3 shows that the proton contains also gluons and other quarks, which give rise to the so-called 'sea' and which exhibit much smaller momenta. They are mainly produced by gluon radiation from the valence quarks, and by subsequent gluon splitting into quark-antiquark pairs.

The parton momentum distributions depend on the 4-momentum exchanged in the interaction (Q^2). At large Q^2, the interacting particles see the short-distance structure of the protons, and hence have access to the sea. Therefore the parton distribution functions are shifted towards small x values. For small Q^2, on the other hand, only the valence quarks are visible and the parton distribution functions peak at large x values.

The cross-section of a generic hard-scattering interaction is given by:

$$\sigma = \sum_{a,b} \int dx_a dx_b f_a(x, Q^2) f_b(x, Q^2) \hat{\sigma}_{ab}(x_a, x_b)$$

where $\hat{\sigma}_{ab}$ is the cross-section of the elementary interaction between the two partons, and the parton distribution functions $f_a(x, Q^2)$ and $f_b(x, Q^2)$ give the probability of finding a parton carrying a fraction x of the proton momentum.

4. THE EXPERIMENTAL CHALLENGES

The LHC experiments will have to face two main experimental difficulties, which are discussed below. The first one (the pile-up) is related to the machine luminosity, the second one (the QCD background) to the physics of pp collisions.

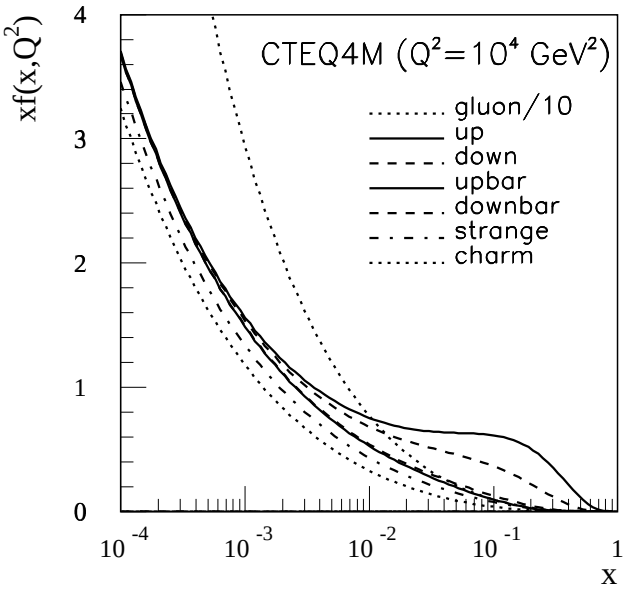

Fig. 3: Parton distribution function of the proton as calculated for $Q^2 = 10^4$ GeV^2.

4.1 Pile-up

Protons are grouped in bunches of $\sim 10^{11}$ protons colliding at a given interaction point every 25 ns. Since the interaction rate is $\sim 10^9$ events/s when running at high luminosity, on average 25 soft interactions (minimum bias events) occur simultaneously at each crossing. These give rise, every 25 ns, to about 1000 charged particles in the detector over the pseudo-rapidity region $|\eta| < 2.5$ [1].

Therefore, when a high-p_T event is produced during a bunch crossing, this event is overlapped, on average, with 25 additional soft events, which are therefore called 'pile-up'.

In order to extract the interesting high-p_T event from the pile-up, one can exploit the fact that particles from minimum-bias events have, as already mentioned, a small p_T. This is illustrated in Fig. 4, which shows an event due to the production of a Higgs boson decaying into four muons, overlapped with 30 minimum-bias events. Before a cut on the p_T of the charged particle tracks is applied, the event is very crowded and the Higgs decay products are not visible. After a loose (2 GeV) p_T cut is applied, the four muon tracks coming from the Higgs boson decay become clearly visible in a much cleaner environment.

The pile-up is one of the most serious difficulties for the experimental operation at the LHC and has had a major impact on the detector design, with three main consequences. First, the LHC detectors must have a fast response time, otherwise the signal from the detector would be integrated over many bunch crossings and therefore the pile-up would be too large. Typical response times of the LHC detectors are in the range 20–50 ns, which corresponds to integrating over 1–2 bunch crossings and therefore summing 25–50 minimum bias events on average. Such a fast response requires sophisticated and highly-performing readout electronics. Furthermore, the LHC detectors must have a fine readout granularity, in order to minimise the probability that particles from the pile-up traverse the same detector element as an interesting object (such as a photon coming from a H $\rightarrow \gamma\gamma$ decay). This implies a large number of electronic channels, and therefore high cost and a challenging detector operation (calibration, monitoring, etc.). Finally, the LHC detectors must be radiation resistant, because there is a high flux of particles coming from the pp collisions. This flux, integrated over ten years of operation, amounts to up to 10^{17}

[1] The pseudo-rapidity η is defined as $\eta = -\ln\cot\theta/2$ where θ is the polar angle of a produced particle with respect to the beam line.

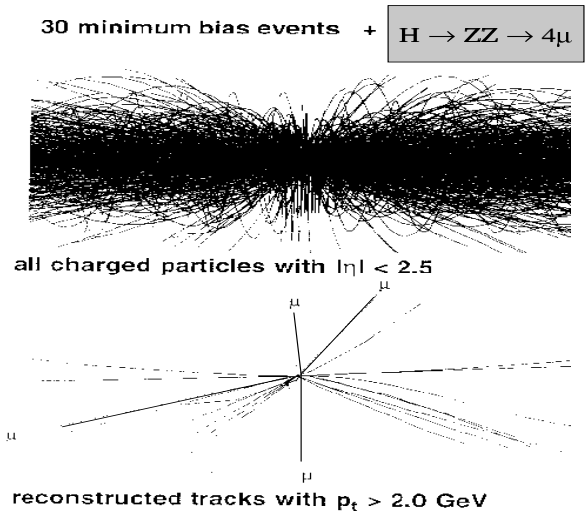

Fig. 4: Simulation of a H$\rightarrow$ 4μ event in the CMS inner detector overlapped with 30 minimum-bias events. Top: all charged particles are shown. Bottom: only reconstructed tracks with $p_T > 2$ GeV are shown.

neutrons/cm^2 and up to 10^7 Gy (1 Gy = 1 Joule/Kg is the unit of absorbed energy) in the forward calorimeters. Such huge particle fluxes can damage the detector composition (e.g. modify the lattice structure of a crystal) and therefore lead to a reduction of the collected signal and, in the worst case, to a detector break-down. Every piece of detector material needs therefore to pass severe quality controls.

4.2 QCD background

The rate of high-p_T events at a hadron collider is dominated by QCD jet production. Jets arise from the fragmentation of quarks and gluons in the final state, which are produced through a variety of Feynman diagrams. An example is shown in Fig. 5 a). Jet production is a strong process and therefore has a large cross-section. Furthermore many channels contribute to this final state (e.g. qq $\rightarrow$ qq, gg $\rightarrow$ qq, qg $\rightarrow$ qg).

On the other hand, the most interesting physics processes at the LHC are rare processes, either because they involve the production of heavy particles, or because they have weak cross-sections (e.g. W production). Figure 6 shows the production cross-sections for several channels at hadron colliders, as a function of the centre-of-mass energy. It can be seen, for example, that at the LHC energy the production cross-section for jets with $p_T > 700$ GeV is five orders of magnitude larger than the cross-section for a Higgs boson of mass 150 GeV. Therefore, there is no hope to detect a Higgs boson decaying into jets (unless it is produced in association with additional particles, see Section 7.1), since such final states are swamped by the much larger jet rate (hereafter referred to as 'QCD background'), and decays to leptons and photons have to be used instead. For the same reasons, and as another example, at LHC there is no hope, unlike at LEP, to observe the production of W pairs with both W bosons decaying into two jets. This process can only be detected if at least one of the two W's decays into leptons.

Since decays into leptons or photons have usually a smaller branching ratio than decays into quarks, the prize to pay to get rid of the QCD background is a smaller event rate.

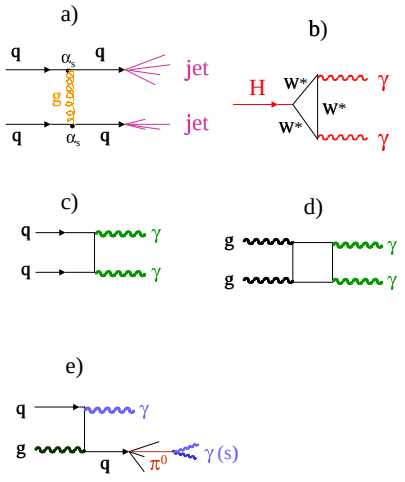

Fig. 5: Examples of Feynman diagrams contributing to various processes: a) QCD production of two jets; b) Higgs boson decay into two photons; c) and d) $\gamma\gamma$ production through the Born and box processes; e) γ-quark production, with the quark fragmenting into a hard isolated π^0.

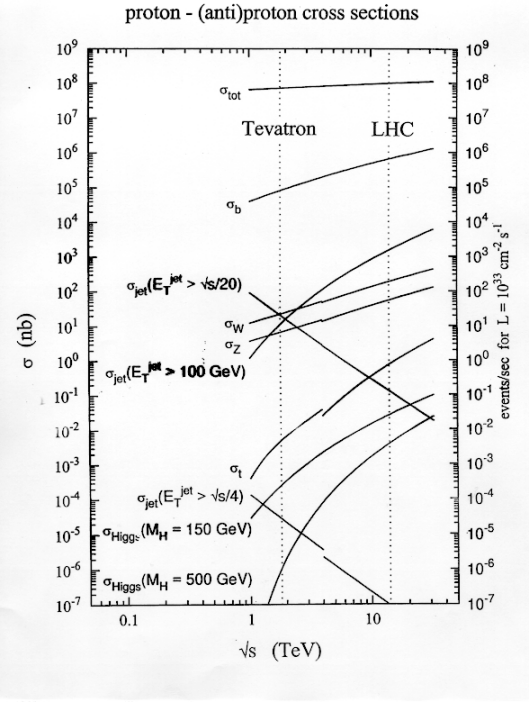

Fig. 6: Production cross-sections for various hard-scattering processes at hadron colliders (pp and $p\overline{p}$), as a function of the machine centre-of-mass energy.

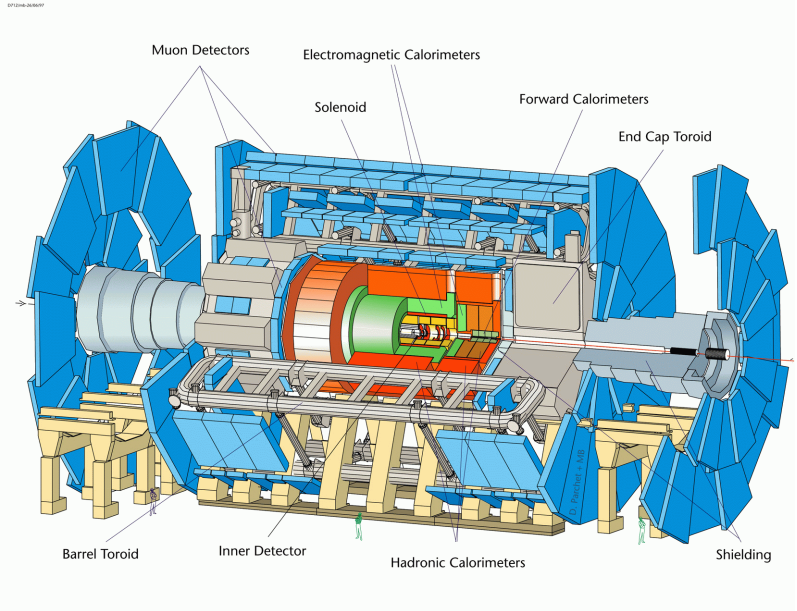

Fig. 7: Overall layout of the ATLAS detector.

5. ATLAS AND CMS

Since it is not known how new physics (if any ...) will manifest, it is mandatory for the LHC experiments to be able to detect as many particles and signatures as possible. ATLAS (A Toroidal Lhc ApparatuS, Fig. 7) and CMS (Compact Muon Solenoid, Fig. 8) are multi-purpose detectors which should allow efficient and precise measurements of electrons, muons, taus, neutrinos, photons, jets, b-jets, etc..

Their layout is similar to that of past and present collider experiments. From the interaction point outwards they consist of: an inner detector immersed in a magnetic field, used to detect charged particles and to measure their momenta and charge, as well as to detect secondary vertices (e.g. from b-quark decays); an electromagnetic calorimeter, which measures the energy and position of electrons and photons and contributes to their identification; a hadron calorimeter, used to measure the energy and position of hadrons and jets, as well as the total event missing transverse energy (see below); a muon spectrometer, used to identify muons and to measure their momentum together with the inner detector.

The main performance requirements of ATLAS and CMS can be summarised as follows:

- Leptons should be measured over the p_T range from a few GeV up to a few TeV. This is needed on the one hand to detect the soft leptons produced in the decays of B-hadrons, and on the other hand to look for heavy particles decaying into leptons (e.g. additional gauge bosons W' and Z') up to masses of ~ 5 TeV.
- Calorimetry should be as hermetic as possible, and cover the full azimuthal angle and the pseudo-rapidity region $|\eta| \leq 5$ (i.e. down to 1° from the beam axis). This is required mainly for a reliable measurement of the event transverse energy, which is in turn needed to detect neutrinos. Neutrinos are weakly interacting particles which can only be detected indirectly by observing a significant amount of missing transverse energy in the final state.
  At $\mathrm{e^+e^-}$ colliders the presence of a neutrino in an event, and the neutrino energy, are simply deduced by comparing the total energy measured in the final state with the centre-of-mass energy of the colliding beams and by applying energy conservation criteria. At hadron colliders, on the other hand, the energy of the interacting quarks and gluons is not known (only the proton energy is known), and therefore the missing energy in the final state cannot be determined. However, since the transverse momentum (perpendicular to the beam axis) of the incident quarks and gluons is

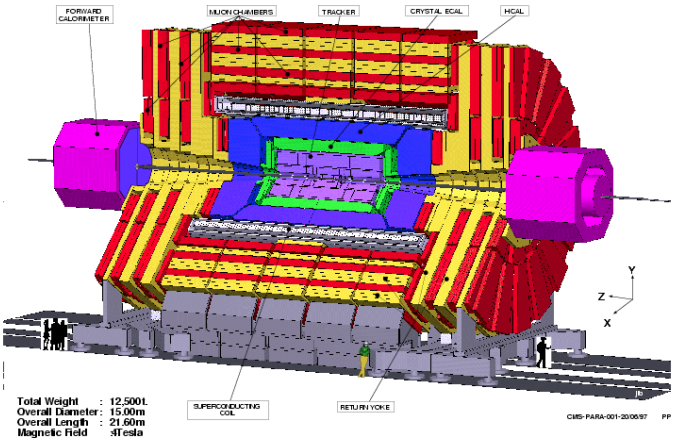

Fig. 8: Overall layout of the CMS detector.

negligible, the total transverse momentum in the initial state is close to zero, and so has to be the total transverse energy in the final state. This constraint is used to detect the presence of neutrinos. In order to minimise energy losses in poorly-instrumented regions of the apparatus, which could fake a neutrino signal, the calorimeters have to cover as much of the solid angle as possible. A large calorimetric coverage is also needed to detect the forward jets produced in association with a heavy Higgs boson [2, 3].

- Excellent mass resolution ($\sim 1\%$) for particles of masses up to a few hundreds GeV decaying into photons, electrons or muons. This is needed, for instance, to extract a Higgs boson signal in the $\gamma\gamma$ decay mode over the irreducible $\gamma\gamma$ background (see Section 7.2). Since the cross-sections for the irreducible backgrounds are often much larger than the signal cross-sections, the reconstructed mass spectrum of the signal particle must be narrow enough to allow observation of a clear resonance above the continuum.
- Several stringent requirements on the identification of electrons, photons, b-jets, taus, etc. must be satisfied. In particular, excellent electron/jet and photon/jet separation capabilities are needed. Jets faking photons should be rejected by a factor of $\sim 10^3$, for a photon efficiency of $\sim$80%, in order to observe a possible H $\rightarrow \gamma\gamma$ signal over the background (Section 7.2).
  The ratio (e/jet) between the inclusive rate of electrons and the inclusive rate of jets with $p_T > 20$ GeV is e/jet $\simeq 10^{-5}$ at the LHC. Therefore jets faking electrons should be rejected by a factor of $\sim 10^6$ in order to observe a clean inclusive electron signal above the QCD background. This same ratio is e/jet $\simeq 10^{-3}$ at the Tevatron $\mathrm{p\overline{p}}$ collider ($\sqrt{s}$ = 2 TeV), which indicates that the particle identification capabilities of ATLAS and CMS must be two orders of magnitude better than those of the Tevatron experiments CDF and D0.
- Triggering at LHC will be much more difficult that at present machines. The interaction rate of 10^9 events/s must be reduced to ~ 100 recorded events per second, which is an affordable data storage rate. Therefore, a very selective and at the same time efficient trigger, providing a rejection of $\sim 10^7$, is needed.
  The trigger of the ATLAS and CMS experiments will be organised in three levels. The first level, which must cope with the largest input rate, will use the fast signals from the calorimeters and muon spectrometer. The second and third levels will use the information from more sub-detectors. Excellent particle identification capabilities are needed already at the trigger stage, in order to extract

Table 1: Main features of the ATLAS and CMS detectors.

	ATLAS	CMS
Magnets(s)	Air-core toroids + solenoid in inner cavity Calorimeters outside field 4 magnets	Solenoid Calorimeters inside field 1 magnet
Inner Detctor	Si layers (pixels and strips) TRD $\rightarrow$ particle identification B = 2 T $\sigma/p_T \sim 5 \times 10^{-4} p_T(\mathrm{GeV}) \oplus 0.01$	Si layers (pixels and strips) No particle identification B = 4 T $\sigma/p_T \sim 1.5 \times 10^{-4} p_T(\mathrm{GeV}) \oplus 0.005$
EM calorimeter	Lead-liquid argon $\sigma/E \sim 10\%/\sqrt{E(\mathrm{GeV})}$ Longitudinal segmentation	$PbWO_4$ crystals $\sigma/E \sim 2-5\%/\sqrt{E(\mathrm{GeV})}$ No longitudinal segmentation
HAD calorimeter	Fe-scintillator + Cu-liquid argon $> 10\ \lambda$ $\sigma/E \sim 50\%/\sqrt{E(\mathrm{GeV})} \oplus 0.03$	Cu-scintillator $> 5.8\ \lambda$ + tail catcher $\sigma/E \sim 65\%/\sqrt{E(\mathrm{GeV})} \oplus 0.05$
Muon spectrometer	Air $\sigma/p_T \sim 7\%$ at 1 TeV achieved by spectrometer alone	Fe $\sigma/p_T \sim 5\%$ at 1 TeV achieved by combining with inner det.

efficiently the interesting physics signals while reducing the large QCD backgrounds down to acceptable rates.
Since the trigger decision time is of the order of the microsecond, whereas bunch crossing occurs every 25 ns, events will be stored in pipelines while awaiting for the trigger decision.

The main features of the ATLAS and CMS experiments, which are presently under construction, are presented in Table 1. The two experiments are quite complementary.

CMS (Fig. 8) has only one magnet, a big solenoid which houses the inner detector and the calorimeters and which provides a magnetic field of 4 T. ATLAS (Fig. 7) has four magnets: a solenoid sitting in front of the electromagnetic calorimeter and producing a field of 2 T in the inner cavity, and external barrel and end-cap air-core toroids. The magnet layout determines the size, the weight and even the name of both experiments.

The CMS inner detector consists of layers of Pixel detectors and Silicon strip detectors. Thanks to the large magnetic field, excellent momentum resolution is expected (see Table 1). The ATLAS inner detector has also Pixel and Silicon layers close to the interaction region and, in addition, a Transition Radiation Detector (TRD) at larger radii. Due to the smaller magnetic field and somewhat smaller cavity, the expected momentum resolution is a factor of almost three worse than that of CMS. However, the Transition Radiation Detector provides electron/pion separation capabilities.

The CMS electromagnetic calorimeter is a high-resolution homogeneous crystal detector. The ATLAS calorimeter is a lead-liquid argon sampling calorimeter, therefore with a worse intrinsic energy resolution. However, thanks to a very fine lateral and good longitudinal segmentation, the ATLAS calorimeter should allow more robust particle identification capabilities than the CMS calorimeter.

In both experiments the hadronic calorimeters are sampling calorimeters with scintillator or liquid-argon as active medium. The ATLAS calorimeter is expected to provide a better energy resolution because it is thicker (the CMS hadronic calorimeter suffers from space constraints dictated by the external solenoid) and has a better sampling frequency.

Finally, the external muon spectrometer of CMS consists of chamber planes embedded into the iron of the solenoid return joke, where multiple scattering is not negligible. ATLAS has a spectrometer in air, where multiple scattering is minimised, and therefore offers the possibility of good standalone (i.e. without the inner detector contribution) measurements. The expected momentum resolution is better than

10% for muons of p_T = 1 TeV in both experiments. However, this performance is achieved by the muon spectrometer alone in ATLAS, and by combining the information from the muon spectrometer and the inner detector in CMS.

Both experiments are equipped with more than 10^8 electronic channels.

6. THE PHYSICS PROGRAMME

The LHC offers a very rich and ambitious physics programme, whose main goals can be summarised as follows:

- Search for a Standard Model Higgs boson over the full allowed mass range from the experimental limit set by LEP and Tevatron up to the theoretical upper bound of 1 TeV. If such a particle will be found, the LHC should be able to measure its mass and couplings with high precision.
- Search for Supersymmetry and other physics beyond the Standard Model, such as leptoquarks or additional leptons, quarks and gauge bosons, up to masses of ~ 5 TeV.
- Precise measurements of the W mass, of WWγ and WWZ Triple Gauge Couplings, and of the mass, the couplings and the decay properties of the top quark. Several QCD measurements will also be performed, such as the running of the strong coupling constant α_s over an unprecedented range of Q^2.
- Detailed studies of the physics of B-hadrons and of CP-violation in the B-hadron system. These measurements will be performed also (and with better sensitivity for some aspects) by the dedicated LHCb experiment [6].
- Study of the phase transition from hadronic matter to a plasma of deconfined quarks and gluons. It is believed that the inverse transition (plasma $\rightarrow$ hadronic matter) happened in the universe $\sim 10\,\mu$s after the Big Bang. These studies will be performed by the dedicated ALICE experiment [7].

The strongest asset of the LHC are the expected huge event rates. Examples of production rates are shown in Table 2 for known and new particles, and are compared with the full data samples collected (or to be collected) at other machines.

Table 2: For the physics channels listed in the first column, the expected number of events at the production level in each experiment (ATLAS or CMS) per second and in one year when running at low luminosity (10^{33} cm^{-2}s^{-1}). The total event samples collected or to be collected at other machines are given in the last column.

Process	Events/s	Events/year	Events from previous machines
$\mathrm{W} \rightarrow \mathrm{e}\nu$	15	10^8	10^4 LEP, 10^7 Tevatron
$\mathrm{Z} \rightarrow \mathrm{ee}$	1.5	10^7	10^7 LEP
$\mathrm{t\bar{t}}$	0.8	10^7	10^5 Tevatron
$\mathrm{b\bar{b}}$	10^5	10^{12}	10^8 BaBar, Belle
$\tilde{\mathrm{g}}\tilde{\mathrm{g}}$ $m = 1$ TeV	0.001	10^4	–
SM Higgs m_H = 0.8 TeV	0.001	10^4	–
QCD jets $p_T > 200$ GeV	10^2	10^9	10^7 Tevatron

Even in the initial phase at low luminosity, millions of events should be collected every year in most cases. Therefore the LHC can be considered as a factory of all Standard Model particles, as well as of new particles (e.g. SUSY particles) with masses up to the TeV range.

On the other hand, the weakest point of the LHC, compared not only to $\mathrm{e^+e^-}$ machines but also to the Tevatron $\mathrm{p\overline{p}}$ collider, is the already mentioned harsh environment: pile-up at high luminosity and the large QCD backgrounds to many channels. It should be noted that since the cross-section of QCD

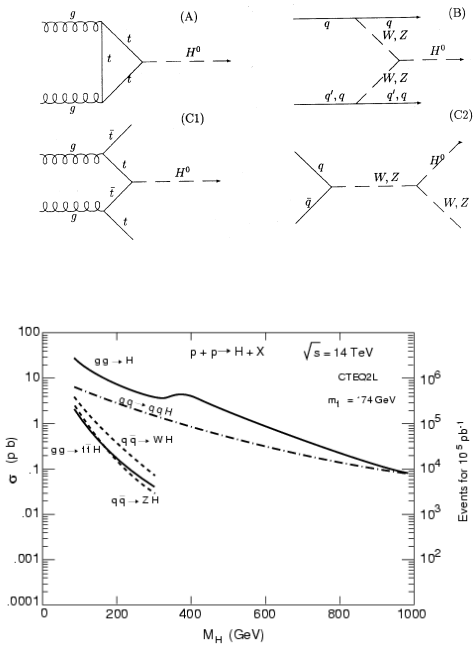

Fig. 9: Top plot: main Feynman diagrams contributing to the production of the SM Higgs boson at the LHC: A) gg-fusion, B) WW and ZZ fusion, C1) associated $\mathrm{t\bar{t}H}$ production, C2) associated WH and ZH production. Bottom plot: expected production cross-section for a SM Higgs boson at the LHC, and number of events for an integrated luminosity of 100 fb^{-1}, as a function of the Higgs mass.

processes grows faster with the centre-of-mass energy than that of electroweak processes (see Fig. 6), the signal-to-background ratio is usually worse at the LHC than at the Tevatron.

A few examples of the LHC physics potential are discussed in more detail in the next Sections.

7. SEARCH FOR THE STANDARD MODEL HIGGS BOSON

The production of the Standard Model Higgs boson at LHC is expected to proceed mainly through the diagrams shown in Fig. 9. The cross-section for these processes is shown in the same figure as a function of the Higgs mass. Gluon-gluon fusion through a top-quark loop is the dominant production channel for all masses. Vector boson (WW, ZZ) fusion becomes increasingly important with increasing Higgs boson masses, attaining a cross-section similar to that of gluon-gluon fusion for $m_H \sim 1$ TeV. This process leads to the very distinctive signature of two jets emitted at small angle with the beam axis ('forward jets'). The associated Higgs production with a $\mathrm{t\bar{t}}$ pair or a W/Z boson has a significantly smaller cross-section, however gives rise to final states which are relatively easy to extract from the background, thanks to the additional signature (for instance leptons) produced in the decay of the accompanying particles.

It can be seen that the total production cross-section is larger than 100 fb even for Higgs masses as high as 1 TeV. Therefore more than 1000 events are expected to be produced in one year of running at low luminosity and more than 10000 events in one year of running at high luminosity for $m_H \sim 1$ TeV.

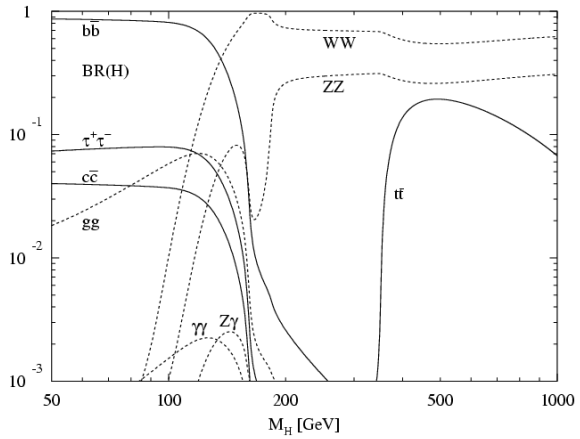

Fig. 10: Branching ratios for the decays of a Standard Model Higgs boson into fermions and bosons as a function of the Higgs boson mass.

The Higgs boson couplings to fermions are proportional to the fermion masses. This is reflected in the decay branching ratios shown in Fig. 10. Three main regions can be identified:

- $m_H < 120$ GeV: the H $\rightarrow \mathrm{b\overline{b}}$ decay mode dominates, since b-quarks are the most massive fermions kinematically accessible in this region.
- 130 GeV $< m_H < 2$ m$_Z$: the decays H $\rightarrow$ WW$^{(*)}$ and H $\rightarrow$ ZZ*, where one of the vector bosons can be virtual, become important and eventually dominate.
- $m_H > 2$ m$_Z$: the Higgs boson decays mainly into WW or ZZ pairs, where both bosons are real.

It should be noted that decays such as H $\rightarrow \gamma\gamma$ are rare, but provide clean signatures against the background.

The Higgs boson width increases with the mass to the third power. For masses of about 100 GeV the Higgs width is of the order of a few MeV, increasing to about 100 GeV for masses of 600 GeV.

7.1 Search strategy

Figure 10 shows that fully hadronic events are the most copious final states expected from a SM Higgs boson production and decay. However, as already mentioned, these events cannot be extracted from the large QCD background, and topologies with leptons and photons have to be exploited instead, despite their smaller branching ratio.

The main channels which will be used at the LHC to look for a Standard Model Higgs boson can be classified as follows:

- Low mass region ($m_H < 130$ GeV). Two decay modes are experimentally important in this region: H $\rightarrow \mathrm{b\overline{b}}$ and H $\rightarrow \gamma\gamma$. The first one has a branching ratio close to 100% in most of this region, and therefore inclusive Higgs production followed by H $\rightarrow \mathrm{b\overline{b}}$ has a large cross-section (~ 20 pb). However, since the signal-to-background ratio for the inclusive production is smaller than 10^{-5}, it will be impossible to observe this channel above the QCD background and even to select it at the trigger level. On the other hand, the associated production $\mathrm{t\overline{t}}$H, WH, ZH, with H $\rightarrow \mathrm{b\overline{b}}$ and with an additional lepton coming from the decay of the accompanying particles, has a much smaller cross section (< 1 pb) but gives rise to final states which can be extracted from the background.
  The H $\rightarrow \gamma\gamma$ channel has a branching ratio at the level of 10^{-3} and therefore a small cross-section (~ 50 fb). However, the signal-to-background ratio ($\sim 10^{-2}$) is much more favourable than for the $\mathrm{b\overline{b}}$ channel.

- Intermediate mass region (130 GeV $\leq m_H < 2$ m$_Z$). The most promising channels for the experimental searches are H $\rightarrow$ WW$^{(*)}$ $\rightarrow \ell\nu\ell\nu$ and H $\rightarrow$ ZZ* $\rightarrow 4\ell$.
- High mass region ($m_H > 2$ m$_Z$). This is the best region to discover a Higgs boson signal at the LHC, since the H $\rightarrow$ ZZ $\rightarrow 4\ell$ channel gives rise to a gold-plated signature, almost background free. For very large masses ($m_H > 500$ GeV) searches for this decay mode will be supplemented by searches for other channels, such as H $\rightarrow$ ZZ $\rightarrow \ell\ell\nu\nu$ and H $\rightarrow$ WW $\rightarrow \ell\nu jj$ (where j stands for jet), which have larger branching ratios and therefore can compensate for the decrease in the production cross-section.

The experimental techniques used to extract a possible signal above the backgrounds and the LHC discovery potential are illustrated here with two examples: the H $\rightarrow \gamma\gamma$ channel and the H $\rightarrow 4\ell$ channel. Detailed discussions of the other channels can be found in [3, 11].

7.2 H $\rightarrow \gamma\gamma$

This channel should allow observation of a Higgs boson over the mass region $80 \leq m_H \leq 150$ GeV. The small branching ratio is due to the fact that the H$\gamma\gamma$ coupling is forbidden at the tree level and therefore the H $\rightarrow \gamma\gamma$ decay occurs only at higher order through a W loop (see Fig. 5 b). The final state consists of two high-p_T photons ($p_T \sim 50$ GeV) with invariant mass compatible with the Higgs boson mass. Despite the simple signature, this is the most challenging channel for the performance of the LHC electromagnetic calorimeters and has indeed driven the design and the technology choices for these detectors. The reason is that there are two large backgrounds to fight:

- $\gamma\gamma$ production, which occurs for instance through the diagrams shown in Fig. 5 (c,d). This is an irreducible background (i.e. it gives rise to exactly the same final state as the signal), which has no resonant structure and decreases smoothly with the invariant mass of the two photons. The $\gamma\gamma$ cross-section is 60 times larger than the H $\rightarrow \gamma\gamma$ cross-section in the region $m_{\gamma\gamma} \simeq 100$ GeV. Therefore, excellent detector energy and angular resolutions are needed in order to extract a narrow resonant peak above the overwhelming continuum background.
- γj and jj production, where one or both jets fake a photon. In general, a jet consists of many particles, and therefore it can be easily recognised from a single photon for instance from the broader shower size in the calorimeters or from the presence of several tracks in the inner detector associated to the calorimeter shower. There are however (rare) cases in which a jet of particles can fake a single photon, as illustrated in Fig. 5 (e). This happens when a quark fragments into a very hard π^0 plus a few other particles which are too soft to be detected. The two photons from the subsequent π^0 decay are very close in space because the parent π^0 is usually produced with a large boost. For instance, for a π^0 of $p_T \sim 50$ GeV the distance between the two decay photons is smaller than 1 cm at 150 cm from the interaction point, which is approximately the radius at which electromagnetic calorimeters are located. Therefore the two photons appear as a single photon in the electromagnetic calorimeter, unless the latter has a fine enough granularity to allow detection of two distinct showers. Although the probability for a jet to fragment into a single isolated π^0 is small, the cross-section for γj and jj production is $\sim 10^6$ times larger than the cross-section for the $\gamma\gamma$ continuum. Therefore a jet rejection of at least 1000 is required in order to suppress this jet background to well below the irreducible $\gamma\gamma$ background.

Excellent performance of the electromagnetic calorimeters is needed to extract a H $\rightarrow \gamma\gamma$ signal from both the aforementioned backgrounds.

As already mentioned, an adequate rejection of the jet background requires electromagnetic calorimeters with fine readout granularity. The CMS crystal calorimeter has a lateral cell size of 2 x 2 cm^2, and the first longitudinal compartment of the ATLAS calorimeter is segmented into narrow strips (4 mm pitch) in the η direction. Figure 11 shows the shower profile in these strips for a single photon and for a $\pi^0 \rightarrow \gamma\gamma$. Two close-by showers are visible in the latter case. Figure 11 shows also the jet rejection

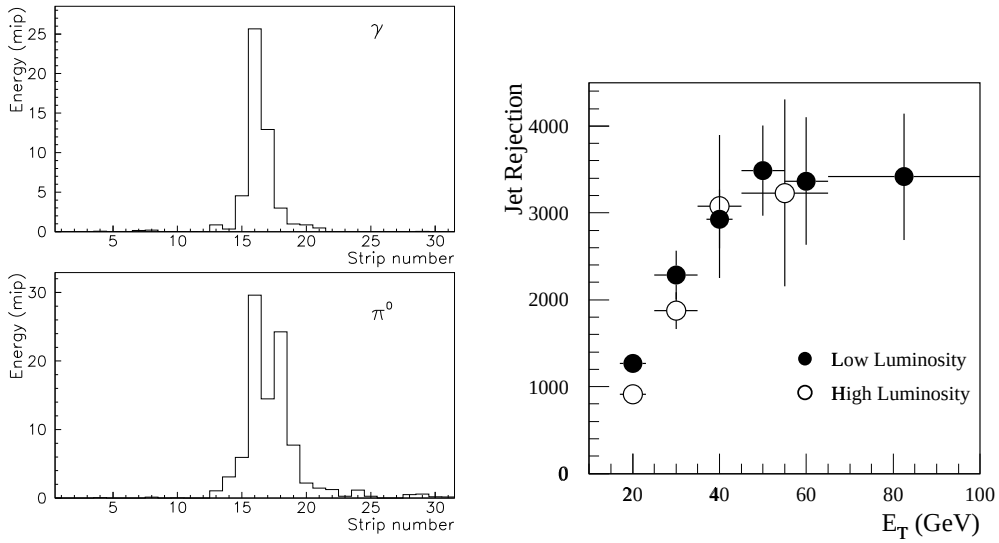

Fig. 11: Left: shower lateral profile in the η-strips of the ATLAS electromagnetic calorimeter from a GEANT-based simulation of a single photon and of a $\pi^0 \to \gamma\gamma$ of p_T = 50 GeV. Right: jet rejection as a function of the jet p_T, as obtained for a photon efficiency of 80% from a simulation of the ATLAS detector.

expected in ATLAS as a function of the jet p_T. By using mainly the information from the electromagnetic calorimeter (shower shape, shower isolation, etc.) a jet rejection of ~ 3000 can be achieved. This allows the jet background to be reduced to less than 30% of the $\gamma\gamma$ irreducible background.

The $\gamma\gamma$ irreducible background can not be reduced by definition. However, a resonant signal can be observed over the the $\gamma\gamma$ continuum if the reconstructed mass peak is narrow enough. The signal significance S, defined as

$$S = N_s/\sqrt{N_b}$$

where N_s and N_b are the number of signal and background events in the region of the peak, depends on the resolution of the reconstructed mass peak (σ_m) as

$$S \sim 1/\sqrt{\sigma_m}$$

Since the Higgs boson resonance is very narrow ($\sim$ MeV) in the mass region relevant to H $\to \gamma\gamma$ searches, the width of the reconstructed peak is completely determined by the resolution of the electromagnetic calorimeters:

$$\frac{\sigma_m}{m} = \frac{1}{\sqrt{2}}\Big(\frac{\sigma(E_1)}{E_1} \oplus \frac{\sigma(E_2)}{E_2} \oplus \frac{\sigma(\psi)}{\tan\psi/2}\Big)$$

The first two terms on the right-hand side of the above equation come from the resolution of the measurements of the two photon energies and the third term comes from the resolution of the measurement of the angle between the two photons (ψ). A mass resolution of $\sim 1\%$ is needed to observe a resonant signal over the $\gamma\gamma$ continuum with adequate signficance.

An additional difficulty arises from the fact that the position of the interaction vertex along the beam line (z-direction) will have a spread of ~ 5.6 cm at the LHC. Therefore the vertex position will not be known precisely enough to be used (together with the shower position in the calorimeter) to measure the photon direction in θ (θ is the photon angle with respect to the beam line). There should be no problem, on

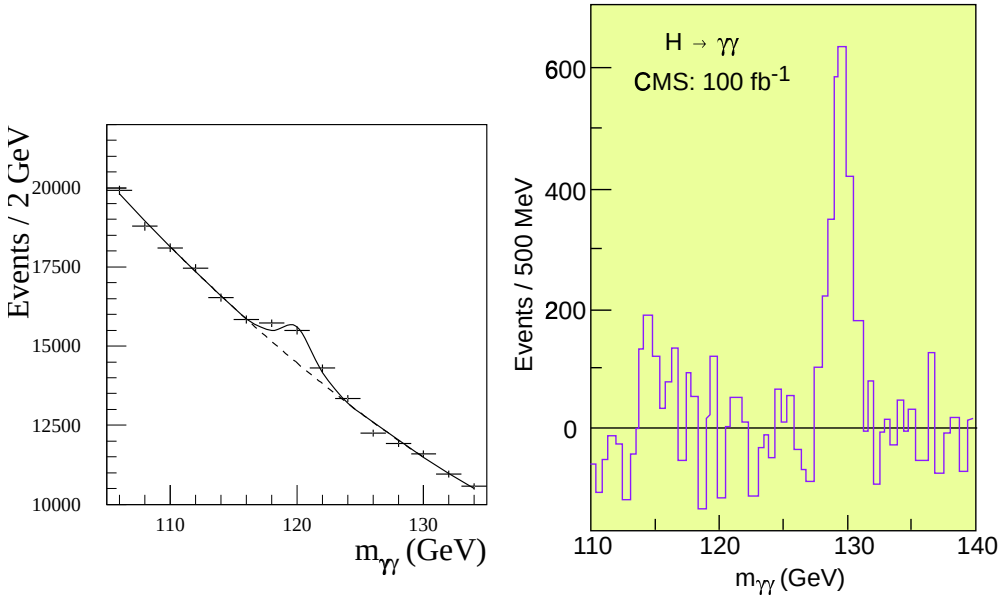

Fig. 12: Expected H $\rightarrow \gamma\gamma$ signal at the LHC for an integrated luminosity of 100 fb^{-1}. Left: the signal reconstructed in ATLAS for m_H = 120 GeV is shown on top of the irreducible $\gamma\gamma$ background. Right: the signal reconstructed in CMS for m_H = 130 GeV is shown after background subtraction.

the other hand, for the measurement of the photon angle ϕ in the transverse plane because in this projection the vertex position is expected to be known to $\sim 15\ \mu$m.

The expected performance of the ATLAS and CMS electromagnetic calorimeters for the detection of a possible H $\rightarrow \gamma\gamma$ signal is quite complementary. The mass resolution expected in ATLAS at high luminosity is about 1.3 GeV for a Higgs mass of $\sim$ 100 GeV, and the reconstruction efficiency for H $\rightarrow \gamma\gamma$ events is about 30%. The photon direction in θ is obtained by using the longitudinal segmentation of the electromagnetic calorimeter, i.e. by measuring the shower z-positions at different depths in the calorimeter. The angular resolution achieved in this way is ~ 50 mrad/$\sqrt{E(\mathrm{GeV})}$. The mass resolution expected in CMS is about 0.7 GeV for a Higgs mass of $\sim$ 100 GeV, thanks to the excellent energy resolution of the crystal calorimeter. However, the reconstruction efficiency for H $\rightarrow \gamma\gamma$ events is expected to be $\sim$20%, i.e. smaller than in ATLAS. The reason is that the CMS calorimeter has no longitudinal segmentation, and hence does not provide a measurement of the shower direction in θ. Therefore, the vertex position will be measured by using the tracks of the underlying event, which is that part of the event produced by the interaction of the spectator partons [2]. However, at high luminosity, when on average 25 interaction vertices will be produced in each collision, the probability of selecting the wrong vertex, and therefore reconstructing a wrong $\gamma\gamma$ mass, is non negligible, leading to some efficiency losses.

Figure 12 shows the expected H $\rightarrow \gamma\gamma$ signal in ATLAS above the continuum $\gamma\gamma$ background, for a Higgs mass of 120 GeV and an integrated luminosity of 100 fb^{-1}, which should be achieved after four years of LHC operation. About 1000 events are expected in the Higgs peak. Also shown is the expected signal in CMS for m_H = 130 GeV, after background subtraction. The signal significance in each experiment should be larger than five for Higgs masses between 110 GeV and 140 GeV and for an integrated luminosity of 100 fb^{-1} per experiment. The CMS significance should be about 15% better than the ATLAS significance, due to the already mentioned better energy resolution of the electromagnetic calorimeter.

[2]The spectator partons are those constituents of the incoming protons which do not participate to the hard-scattering interaction (see Fig. 2). They collide at large distance and give rise to low-p_T particles in the final state, called 'the underlying event'.

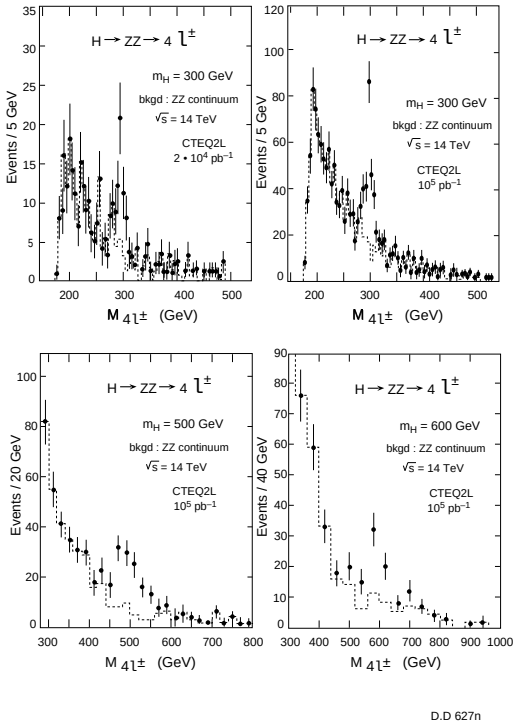

Fig. 13: Expected H $\rightarrow 4\ell$ signal in CMS above the background for various Higgs boson masses and integrated luminosities.

7.3 $\mathbf{H \rightarrow ZZ^{(*)} \rightarrow 4\ell}$

This channel, which can be observed at the LHC over the mass region 120–700 GeV, gives rise to a very distinctive signature, consisting of four leptons (electrons and muons are required, since final states with tau's do not allow clean reconstruction of the Higgs mass peak and are also contaminated by larger QCD backgrounds) whose invariant mass is consistent with the nominal Higgs boson mass.

The expected backgrounds, and therefore the search criteria, depend on the Higgs mass. If $m_H > 2\,\mathrm{m_Z}$, then both Z bosons in the final state are real and two pairs of leptons with same flavour and opposite sign should have an invariant mass compatible with the Z mass. In this region the backgrounds, such as the irreducible pp $\rightarrow$ ZZ $\rightarrow 4\ell$, are small. Furthermore, the intrinsic Higgs width is larger than the experimental mass resolution, therefore the detector performance is not critical. The H $\rightarrow 4\ell$ signal expected in CMS in this mass region is shown in Fig. 13. Clear peaks are visible on top of the background, which become broader with increasing mass due to the increasing Higgs boson width.

For $m_H < 2\,\mathrm{m_Z}$, on the other hand, the backgrounds are large. In addition to the already-mentioned irreducible pp $\rightarrow$ ZZ* $\rightarrow 4\ell$ continuum, there are two potentially dangerous reducible backgrounds: $\mathrm{t\bar{t}} \rightarrow 4\ell$ +X and $\mathrm{Zb\bar{b}} \rightarrow 4\ell$ +X. In the first case, two leptons come from the two W's produced in the t $\rightarrow$ Wb decays and two leptons come from semileptonic decays of the b-quarks. In the second case, two leptons come from the Z decay and two from the b-quark semileptonic decays. These backgrounds can be rejected by asking the invariant mass of at least one lepton pair to be compatible with the Z mass (this cut is efficient against the $\mathrm{t\bar{t}}$ background), by requiring that all leptons be isolated (leptons from b$\rightarrow \ell$X decays are usually non-isolated), and by requiring that all leptons come from the interaction vertex (leptons from b-quark decays are produced at ~ 1 mm from the vertex due to the long B-hadrons lifetime). Figure 14 shows the expected Higgs boson signal in ATLAS in this mass region. The width of the peaks is determined in this case by the detector energy and momentum resolution since in this region the intrinsic Higgs boson width is small.

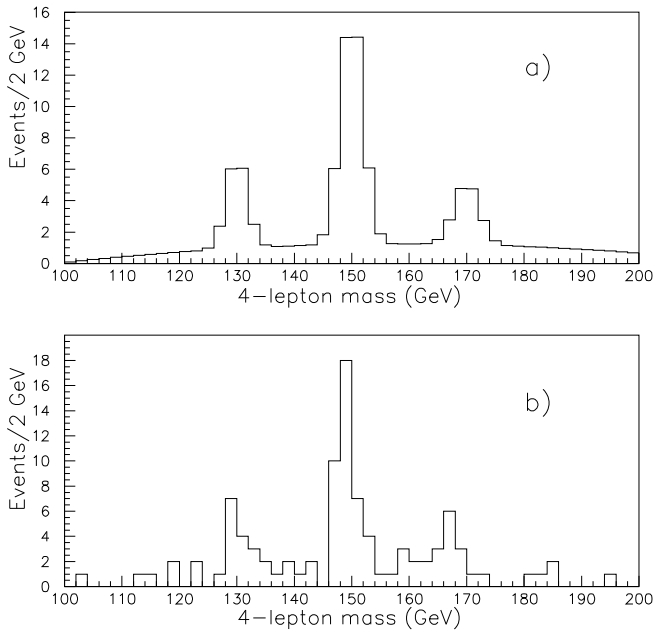

Fig. 14: The reconstructed four-lepton mass above the background as expected in ATLAS for various Higgs boson masses and for an integrated luminosity of 30 fb^{-1}. Plot (a) shows the expected average number of events and plot (b) the result of one experiment obtained with randomized statistics in each mass bin.

The signal significance expected in each experiment varies between three and 25 for an integrated luminosity of 30 fb^{-1} per experiment (which should be collected after three years of data taking at LHC), over the Higgs mass range 120–700 GeV. For larger masses, the production cross-section decreases fast and the width increases, and the branching ratio into four lepton final states is too small to allow observation of this channel.

7.4 Overall discovery potential

The discovery potential for a Standard Model Higgs boson at the LHC is presented in Fig. 15, which shows the signal significance as a function of mass expected in ATLAS for an integrated luminosity of 100 fb^{-1}. Similar results have been obtained by CMS [3].

By combining both experiments, it should be possible to discover a signal at LHC (with significance $S > 5$) over the full allowed mass region from the limit set by previous machines up to the theoretical upper bound of 1 TeV, after less than two years of operation. It can be seen that different channels cover different mass regions, but over most of the mass range more than one channel should be observed, thus giving robustness to the discovery and hints to understand the nature of the signal. As already mentioned, the detector performance in terms of mass resolution, angular coverage, particle identification capability, etc. will be crucial in most cases to achieve these goals.

If a SM Higgs boson will be observed at the LHC, then ATLAS and CMS should be able to measure its mass with a precision of $\sim 0.1\%$ for masses up to ~ 600 GeV [11].

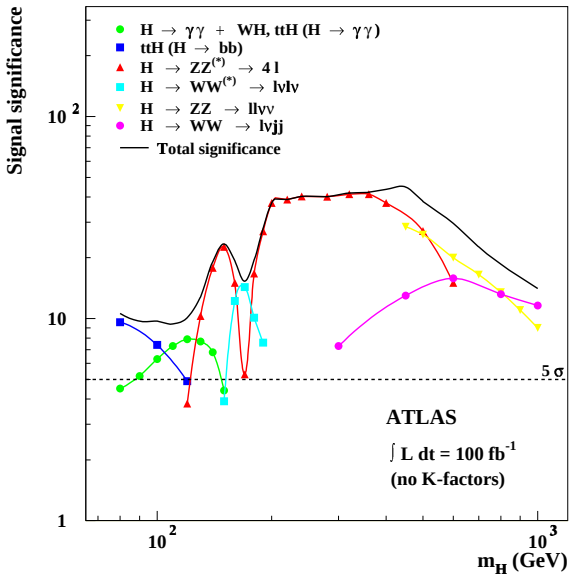

Fig. 15: Expected discovery potential for a Standard Model Higgs boson in ATLAS, as a function of the Higgs boson mass, for an integrated luminosity of 100 fb^{-1}. The different symbols indicate the significance of the different search channels, whereas the full line gives the total significance.

8. SEARCH FOR SUPERSYMMETRY

Supersymmetry is one of the best motivated theoretical scenarios for physics beyond the Standard Model, as discussed in [9]. However, no experimental evidence for SUSY has been found as yet, therefore either SUSY does not exist, or Supersymmetric particles are too heavy ($m >> 100$ GeV) to be accessible at present machines. Since low-energy Supersymmetry predicts a full spectrum of new particles with masses of order 1 TeV or smaller, then the LHC should be able to say the final word about this class of theories.

The LHC discovery potential is discussed here for the most popular theoretical model, that is the Minimal Supersymmetric Extension of the Standard Model (MSSM) with R-parity conservation [9].

The MSSM predicts the existence of a minimal number of additional particles: five Higgs bosons (h, H, A, H$^{\pm}$) and the Supersymmetric partners of ordinary particles, which have a spin different by half-unit compared to their SM partners, and which are listed in Table 3. The masses of these particles are not known, however charginos and neutralinos should be lighter than squarks and gluinos. Present lower

Table 3: Standard Model particles and their Supersymmetric partners.

SM particles	SUSY partners	Examples of physical states
quarks	squarks	$\tilde{u}$, $\tilde{s}$, etc.
leptons	sleptons	$\tilde{e}$, $\tilde{\mu}$, etc.
gluon	gluino	$\tilde{g}$
W bosons charged Higgs bosons	winos charged Higgsinos	mix into 2 charginos $\chi^{\pm}_{1,2}$
Z boson photon neutral Higgs bosons	zino photino neutral Higgsinos	mix into 4 neutralinos $\chi^{0}_{1,2,3,4}$

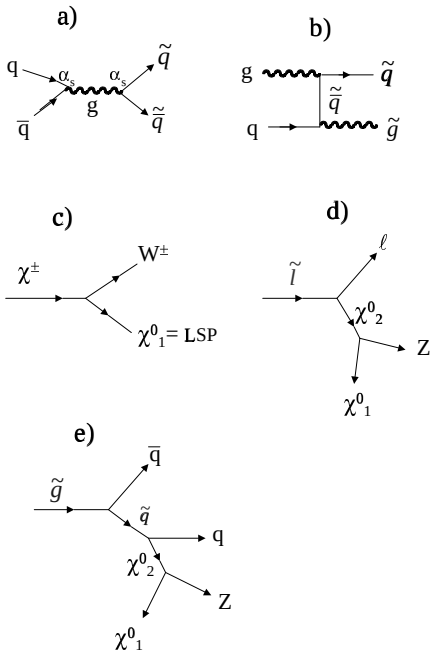

Fig. 16: Examples of Feynman diagrams contributing to: $\tilde{q}$ and $\tilde{g}$ production (a, b); chargino decay (c); slepton decay (d); gluino decay (e).

limits on the chargino and slepton masses are in the range 90–100 GeV (from LEP), whereas limits on squarks and gluino masses are at the level of 250 GeV (from Tevatron). R-parity is a multiplicative quantum number of value $+1$ for ordinary particles and -1 for SUSY particles. If R-parity is conserved, then SUSY particles are produced in pair and the Lightest Superymmetric Particle (LSP), in most models identified with the lightest neutralino χ_0^1, is stable. The LSP is weakly interacting (for cosmological reasons, i.e. in order to be a good candidate for dark matter) and therefore, as neutrinos, can only be detected indirectly by measuring the event missing transverse energy. The latter is the most typical signature predicted by SUSY theories.

Squarks and gluinos, if kinematically accessible, are expected to be copiously produced at hadron colliders via strong processes. The Feynman diagrams which contribute to the production of $\tilde{q}\tilde{q},\ \tilde{g}\tilde{g},\ \tilde{q}\tilde{g}$ pairs are similar to those contributing to the production of quarks and gluons. Examples are shown in Fig. 16 (a,b). For squark or gluino masses of 1 TeV, the pair production cross-section is about 1 pb at $\sqrt{s}$ = 14 TeV, therefore about 10000 events should be produced in one year of data taking at low luminosity. On the other hand, the pair production of charginos, neutralinos and sleptons, which proceeds through electroweak interactions, has a much smaller rate.

The decay modes of SUSY particles depend on the model parameters, namely particle masses, couplings, etc.. Some typical examples are given in Fig. 16 (c, d, e). Charginos can decay into a W boson plus the LSP, neutralinos into a Z boson plus the LSP, sleptons into leptons plus the LSP. Squarks and gluinos, which are quite heavy given the present experimental limits, give rise to more complicated decay chains consisting of several steps (Fig. 16 e). These cascade decays produce final states containing leptons, many jets, W and Z bosons, sometimes b-quarks and even top-quarks, plus missing transverse energy from the escaping LSP. Furthermore, the decay products have usually large p_T since they originate from heavy

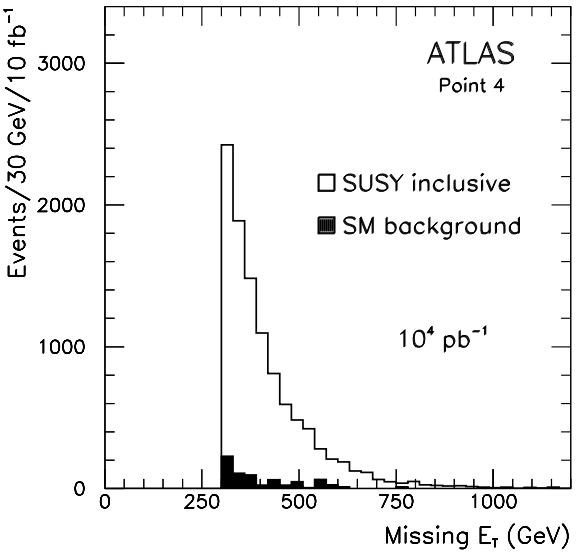

Fig. 17: Distribution of the reconstructed event missing transverse energy as expected in ATLAS for an inclusive SUSY signal (white histogram) and the Standard Model background (shaded area) and for an integrated luminosity of 10 fb^{-1}. The SUSY signal corresponds to the model described in the text.

particles. Such spectacular signatures are therefore quite easy to extract from the Standard Model background. As an example Fig. 17 shows the reconstructed missing transverse energy distribution expected in ATLAS for the Standard Model background and for a SUSY model where the squark mass is 900 GeV, the gluino mass is 600 GeV and the LSP mass 80 GeV. The events have been selected by requiring five high-p_T jets in the final state (with minimum p_T between 90 GeV and 150 GeV) and missing transverse energy larger than 300 GeV. In one year of data taking at low luminosity, about 12000 SUSY signal events are expected after these cuts and 600 events from the SM background. Such a large signal significance is not peculiar of the chosen point in the parameter space, but a rather general feature of the observability of SUSY models with R-parity conservation at the LHC. With similar analyses it should be possible to discover (or exclude) squarks and gluinos with masses up to 1.5–2 TeV in only one year of data taking at low luminosity.

If SUSY will be discovered, many precise measurements of the SUSY particle masses should be possible at the LHC [11]. This should allow the parameters of the underlying theory to be constrained with precisions at the level of the percent for minimal models such as minimal Supergravity [11].

9. MEASUREMENT OF THE W MASS

The W mass is a fundamental parameter of the Standard Model, related to other parameters of the theory, such as the electromagnetic coupling constant α_{EM}, the Fermi constant G_F and the Weinberg angle $\sin\theta_W$, through the relation

$$m_W = \left(\frac{\pi\alpha_{EM}}{\sqrt{2}G_F}\right)^{1/2} \frac{1}{\sin\theta_W\sqrt{1-\Delta r}}$$

where Δr accounts for the radiative corrections, which amount to 4% and depend on the top mass as $\sim m^2_{\rm top}$ and on the Higgs mass as $\sim \ln m_H$. Since α_{EM}, G_F and $\sin\theta_W$ are all known with high accuracy [12], precise measurements of both the top mass and the W mass allow constraints to be put on the

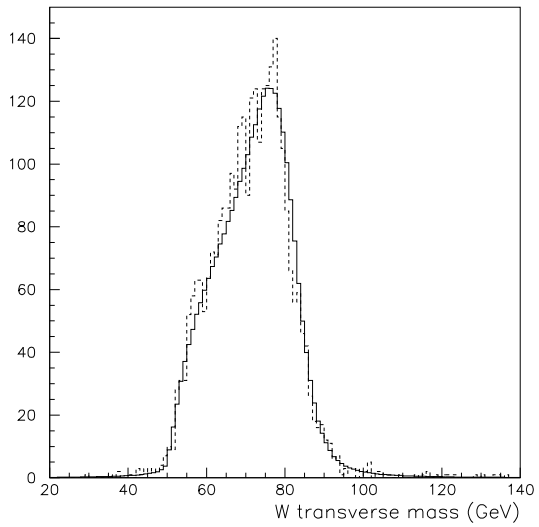

Fig. 18: Distribution of the reconstructed transverse mass as expected in ATLAS for a W mass of 80.3 GeV (full line). The distribution for a mass of 79.8 GeV is also shown (dashed line) for the purpose of illustration.

Higgs boson mass. These constraints are unfortunately relatively weak given the logarithmic dependence of Δr on the Higgs boson mass.

In the year 2005, at the time of the LHC start-up, the W mass will be known with a precision of $\sim$ 30 MeV from measurements at LEP [13] and Tevatron Run 2 [14]. Thanks to the high-statistics data samples, the LHC should be able to improve on these results, and therefore to provide more stringent tests of the underlying theory.

At hadron colliders the measurement of the W mass is performed in the W $\rightarrow$ eν and W $\rightarrow \mu\nu$ channels, since the W $\rightarrow jj$ channel can not be extracted above the QCD background and the W $\rightarrow \tau\nu$ channel is poorly constrained due to the presence of three neutrinos.

The invariant mass of the $\ell\nu$ system can not be reconstructed because the longitudinal momentum of the neutrino is not known (only the transverse momentum is accessible through the measurement of the event missing transverse energy). Therefore the transverse mass m_T^W is used instead, which is the invariant mass of the $\ell\nu$ system evaluated in the plane transverse to the beam:

$$m_T^W = \sqrt{p_T^\ell p_T^\nu (1 - \cos\Delta\phi)}$$

The transverse momentum of the neutrino p_T^ν is obtained from the transverse momentum of the lepton p_T^ℓ and the transverse momentum $\overline{u}$ of the system recoiling against the W (hereafter called 'the recoil'). $\Delta\phi$ is the angle between the electron and the neutrino in the transverse plane.

The transverse mass distribution, and in particular its trailing edge, is sensitive to the value of the W mass, as illustrated in Fig. 18. Therefore, by fitting the experimental distribution of the transverse mass with Monte Carlo samples generated with different values of m_W, it is possible to obtain the mass which best fits the data.

At the LHC, the W boson will be mainly produced via quark-antiquark annihilation (e.g. $u\overline{d}$) with a cross-section of about 150 nb. Sixty million well-reconstructed W $\rightarrow \ell\nu$ decays (where ℓ = e or ℓ = μ) should be selected by each experiment in one year of data taking at high luminosity. Therefore, the statistical error on the mass measurement is expected to be small (< 2 MeV).

The systematic uncertainties will come mainly from the Monte Carlo reliability in reproducing the data in terms of physics and detector performance. Uncertainties related to the physics are for instance the limited knowledge of the p_T spectrum of the W, of the parton distribution functions, of the W width and of the radiative decays $W \to \ell\nu\gamma$. Uncertainties related to the detector are for instance the knowledge of the lepton energy scale, of the lepton energy resolution and of the detector response to the recoil.

Preliminary estimates of the expected uncertainties on the W mass measurement in ATLAS, based in part on extrapolating from the present Tevatron results, are presented in Table 4.

Table 4: Expected contributions to the uncertainty on the W mass measurement in ATLAS for each lepton family and for an integrated luminosity of 10 fb^{-1} (fourth column). The corresponding uncertainties obtained by the CDF experiment in the electron channel in Run 1A [15] and Run 1B [16] are shown for comparison (second and third column). Units are MeV.

SOURCE	Δm_W (CDF Run 1A)	Δm_W (CDF Run 1B)	Δm_W (ATLAS)
Statistics	145	65	< 2
Energy and momentum scale	120	75	15
Energy and momentum resolution	80	25	5
Recoil model	60	33	5
Lepton identification	25	–	5
p_T^W	45	20	5
Parton distribution functions	50	15	10
W width	20	10	7
Radiative decays	20	20	< 10
Background	10	5	5
TOTAL	230	113	< 25

As it is the case today at the Tevatron, at the LHC the dominant uncertainty will most likely come from the calibration of the absolute lepton energy and momentum scale. If such a scale is known to 1%, this translates into an equivalent fractional uncertainty on the W mass, i.e. $\sim$ 80 MeV. Therefore, to achieve a precision of $\sim$ 20 MeV, needed to improve on the LEP and Tevatron ultimate accuracy, the lepton scale should be known to 0.02%, which represents the most serious experimental challenge in this measurement.

The lepton scale will be determined *in situ* at the LHC by using mainly large statistics samples of $Z \to \ell\ell$ decays, which should allow calibration of the muon momentum measured in the inner detector and in the muon spectrometer and of the electron energy measured in the calorimeter by imposing that the invariant mass of the two leptons be compatible with the Z mass. About one $Z \to \ell\ell$ decay per second and per lepton family is expected to be produced at the LHC in the initial phase at low luminosity. The Z boson has the davantage of being a resonance very close in mass to the W, therefore the extrapolation error between the mass region where the calibration is performed and the region where the measurement is performed is small. Today at the Tevatron the lepton scale is known with a precision of about 0.1% [16], dominated by the limited statistics of the Z sample. Preliminary studies [17] indicate that a precision of 0.02% will be difficult to achieve at the LHC but not impossible.

All other systematic uncertainties in Table 4 are expected to be smaller than 10 MeV. Therefore, by combining both channels (electron and muon) and both experiments (ATLAS and CMS) it should be possible to obtain a total error of $\sim$15 MeV. This remains, however, a very difficult and challenging measurement, as discussed in more detail in Ref. [11].

10. MEASUREMENT OF THE TOP MASS

The top quark is the most intriguing fermion, because of its large mass, its large width (which makes it decay before hadronising) and the special rôle it plays in the radiative corrections (see Section 9.). Pre-

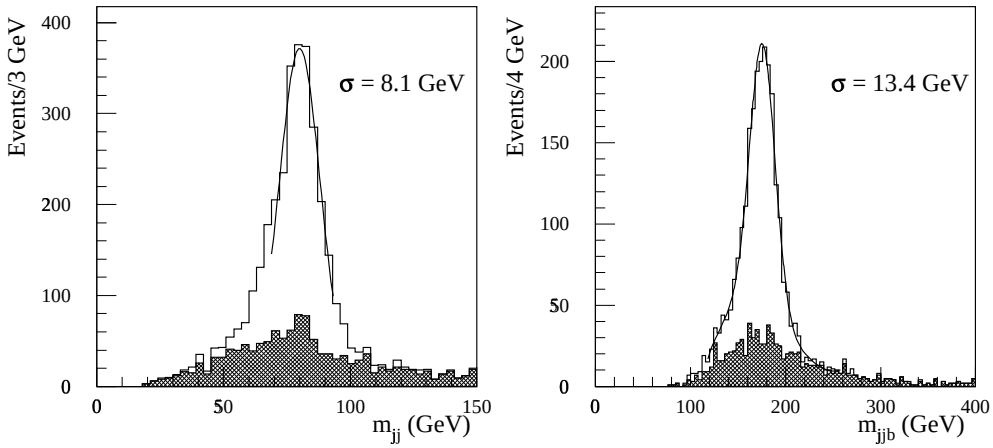

Fig. 19: Distributions of the reconstructed invariant masses of the jj system (left) and jjb system (right), as obtained from the full simulation of a sample of $\mathrm{t\bar{t}}$ events in the ATLAS detector. The black histogram is the background and the white histogram is the sum of the signal and of the background.

cision measurements in the top sector could therefore be important to get more clues on the origin of the fermion mass hierarchy.

Measurements of the top properties have recently begun at the Tevatron [18]. At the LHC, these measurements will benefit from a very large statistics. The production cross-section of $\mathrm{t\bar{t}}$ pairs (mainly via gluon-gluon fusion) is about 800 pb, which is a factor of $\sim$100 times larger than at the Tevatron energies. About eight million $\mathrm{t\bar{t}}$ pairs should be produced in each experiment in one year of running at low luminosity, which should allow precise measurements to be performed of the top production cross-section, mass, branching ratios, couplings, rare decays, etc.

It should also be noticed that $\mathrm{t\bar{t}}$ production is expected to be one of the main backgrounds to many new physics channels (Higgs and SUSY searches, for instance), therefore a very precise knowledge of this process is mandatory. Furthermore, this sample will be used to calibrate *in situ* the jet energy scale, as discussed below.

The best channel to measure the top mass at hadron colliders is $\mathrm{t\bar{t}}$ production where one top decays semileptonically ($\mathrm{t} \rightarrow \mathrm{Wb} \rightarrow \ell\nu\mathrm{b}$, where $\ell = \mathrm{e}$ or $\ell = \mu$) and the other one hadronically ($\mathrm{t} \rightarrow \mathrm{Wb} \rightarrow \mathrm{jjb}$). These events can be selected by requiring one lepton with p_T >20 GeV (which is also used to trigger the experiment), missing transverse energy larger than 20 GeV (because of the presence of a neutrino), two jets tagged as b-jets and two additional jets. The invariant mass distribution of these latter jets (m_{jj}) obtained from the full simulation of a sample of $\mathrm{t\bar{t}}$ events in the ATLAS detector, is shown in Fig. 19 (left-hand plot). A clear peak is visible at the W mass. The mass resolution is $\sim$ 8 GeV. Only events with an invariant mass m_{jj} compatible with the W mass are further considered. The jj pair is then combined with a b-jet to reconstruct the top mass. Since there are two b-tagged jets in the event, the ambiguity can be solved by selecting for instance the jjb combination which gives the largest p_T of the reconstructed top-quark. The invariant mass distribution of the selected jjb combination is shown in Fig. 19 (right-hand plot). A clean peak at the nominal top quark mass is visible. The mass resolution is about 13 GeV.

The expected uncertainties on the measurement of the top mass at the LHC are listed in Table 5. They arise from the limited knowledge of: the jet energy scale, the b-fragmentation mechanism, the initial and final state gluon radiation by the incoming or outgoing quarks and the background.

Table 5: Expected contributions to the uncertainty on the top mass measurement in ATLAS for an integrated luminosity of 10 fb^{-1}.

SOURCE	$\Delta m_{\rm top}$ (GeV)
Statistics	< 0.07
Light-jet scale	0.3
b-jet scale	0.7
b-fragmentation	0.3
Initial State Radiation	0.3
Final State Radiation	1.2
Background	0.2
TOTAL	$\sim$1.5 GeV

The precision on the jet energy scale depends not only on the detector (calorimeters) calibration but also on the knowledge of the physics (quark fragmentation, gluon radiation, etc.). The LHC goal is to achieve an uncertainty of 1% or better on both the scale of light quarks (u, d, s, c) and the scale of b-quarks, by performing *in situ* calibration with physics samples [17]. In particular, W $\rightarrow jj$ decays from $\rm t\bar{t}$ events will be used to calibrate the light-quark jet scale, since these final states are very clean and are the same used to measure the top mass, which avoids any extrapolation error. The b-jet scale will most likely be determined by using samples of Z bosons accompanied by one b-jet, with the Z decaying into ee or $\mu\mu$ pairs, and by requiring p_T balance between the well-measured Z boson and the b-jet.

Another dominant error is the knowledge of final state gluon radiation (FSR). This is due to the fact that jets are reconstructed in cones of limited size (for $\rm t\bar{t}$ final states cones of half-angle $\Delta R = \sqrt{\Delta\phi^2 + \Delta\eta^2} = 0.7$ will most likely be used). Therefore a gluon radiated by a quark may not be fully contained in the cone used to reconstruct the jet associated to that quark. These out-of-cone energy losses lead to an under-estimate of the energy of the initial quark and therefore to shifts in the reconstructed top-quark mass. These shifts are larger the smaller the cone size [3]. Corrections can be applied, but the uncertainty on the FSR mechanism (e.g. coming from the uncertainty on the value of the strong coupling constant α_s) translates into an error on the measured top mass.

In conclusion, the top mass should be measured at the LHC with a precision of ~ 1.5 GeV per experiment after only one year of data taking. This represents an improvement by a factor of almost two on the ultimate Tevatron sensitivity of 2–3 GeV [14]. It should be noted that in this case, and unlike for the W mass, the precision will most likely be limited by the knowledge of the physics and not by the knowledge of the detector performance.

A discussion of other methods for measuring the top mass at the LHC and of the precision expected on the measurements of other properties of the top quark can be found in Refs. [3, 11].

11. CONCLUSIONS

Thanks to the large centre-of-mass energy and high luminosity of the machine, the LHC project offers a very broad and ambitious physics programme, and could improve (and maybe modify) our understanding of the physics of elementary particles and their interactions.

The sensitivity to new physics (e.g. Higgs bosons, Supersymmetry and other theories beyond the Standard Model) includes a large number of topologies and scenarios and extends up to particle masses of ~ 5 TeV. In particular, the Standard Model Higgs mechanism and the low-energy Supersymmetry can be definitely excluded if no evidence will be found at the LHC.

[3] On the other hand, if too large cones were used, then energy coming from the rest of the event and not belonging to the jet would be collected in the cone, leading this time to an over-estimate of the initial quark energy.

The huge discovery potential is complemented by the possibility of performing several precise measurements in many sectors (e.g. W and Z physics, Triple Gauge Couplings, top and B-physics). In most cases, significant improvements on the results obtained at previous machines are expected.

References

[1] D. Boussard et al., The Large Hadron Collider conceptual design, CERN/AC/95–05 (1995).

[2] ATLAS Collaboration, ATLAS Technical Proposal, CERN/LHCC/94–43 (1994).

[3] CMS Collaboration, CMS Technical Proposal, CERN/LHCC/94–38 (1994).

[4] LHCb Collaboration, LHCb Technical Proposal, CERN/LHCC/98–4 (1998).

[5] ALICE Collaboration, ALICE Technical Proposal, CERN/LHCC/95–71 (1995).

[6] P. Harrison, these proceedings.

[7] K. Safarik, these proceedings.

[8] LEP Higgs Working Group, Searches for Higgs bosons: preliminary combined results using LEP data collected at energies up to 202 GeV, ALEPH Note 2000-028, DELPHI Note 2000-050, L3 Note 2525, OPAL Note TN646, March 2000.

[9] M. Carena, these proceedings.

[10] U. Amaldi, W. de Boer and H. Fürstenau, Phys. Lett. **260B** (1991) 447.

[11] ATLAS Collaboration, Detector and Physics Performance Technical Design Report, Vol. 2, CERN/LHCC/99–15 (1999).

[12] C. Caso at al. (Particle Data Group), Eur. Phys. J. C3 (1998) 1.

[13] G. Altarelli, T. Sjöstrand and F. Zwirner, Physics at LEP2, CERN 96–01 (1996).

[14] D. Amidei and R. Brock, Future electroweak physics at the Fermilab Tevatron, FERMILAB-PUB-96/082 (1996).

[15] CDF Collaboration, Phys. Rev. **D52** (1995) 4784.

[16] R. Wagner, Electroweak physics at the Tevatron, talk given at the LHCC Standard Model Workshop, CERN May 25th 1999, http://home.cern.ch/ mlm/lhc99/may25prog.html.

[17] ATLAS Collaboration, Detector and Physics Performance Technical Design Report, Vol. 1, CERN/LHCC/99–14 (1999).

[18] P.C. Bhat, H.B. Prosper and D.D. Sneyder, FERMILAB-PUB-98/236.